JCI The Journal of Clinical Investigation

# Sonic Hedgehog repression underlies gigaxonin mutation-induced motor deficits in giant axonal neuropathy

Yoan Arribat, … , Mireille Rossel, Pascale Bomont

*J Clin Invest.* 2019. https://doi.org/10.1172/JCI129788.

Research In-Press Preview Neuroscience

## Graphical abstract

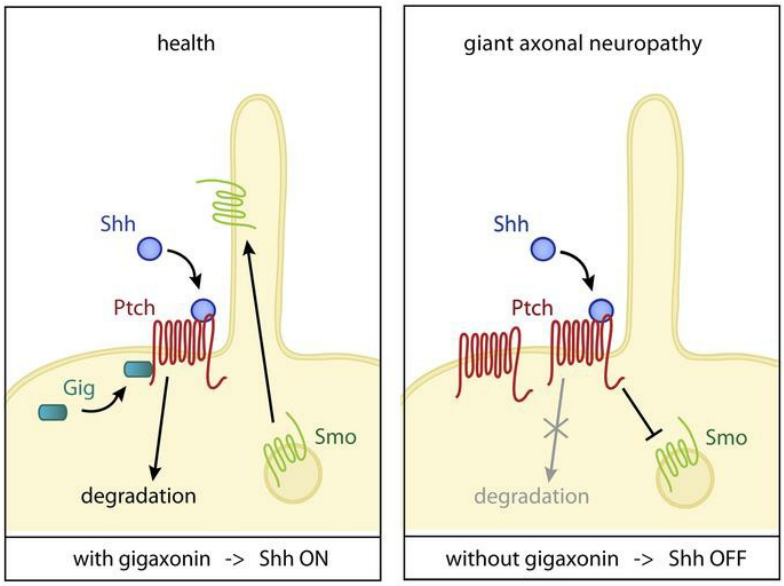

**Title:**

# Sonic Hedgehog repression underlies gigaxonin mutation-induced motor deficits in giant axonal neuropathy

Yoan Arribat[1,2,$], Karolina S. Mysiak[1,$], Léa Lescouzères[1], Alexia Boizot[1,3], Maxime Ruiz[1,4], Mireille Rossel[5] and Pascale Bomont[1*]

[$] Co-first authors, equal contribution, placed in alphabetical order

[1] ATIP-Avenir team, INM, INSERM, University Montpellier, Montpellier, France

[2] present address: UNIL-DP, Bugnon 7, 1005 Lausanne, Switzerland

[3] present address: EDM-CHUV, Bugnon 07, 1005 Lausanne, Switzerland

[4] present address: JSEI, UCLA, Los Angeles, California

[5] MMDN, Univ. Montpellier, EPHE, INSERM, U1198, PSL Research University, Montpellier, France

[*] Correspondence and lead contact: Pascale Bomont, INM-INSERM U1051, Hopital St Eloi, 80 Rue A. Fliche BP 74103, 34091 Montpellier, France. Email: pascale.bomont@inserm.fr; Phone: 33 4 99 63 60 73

## CONFLICT OF INTEREST STATEMENT

The authors have declared that no conflict of interest exists

**ABSTRACT**

Growing evidence shows that alterations occurring at early developmental stages contribute to symptoms manifested in adulthood in the setting of neurodegenerative diseases. Here, we studied the molecular mechanisms causing giant axonal neuropathy (GAN), a severe neurodegenerative disease due to loss-of-function of the gigaxonin-E3 ligase. We showed that gigaxonin governs Sonic Hedgehog (Shh) induction, the developmental pathway patterning the dorso-ventral axis of the neural tube and muscles, by controlling the degradation of the Shh-bound Patched receptor. Similarly to Shh inhibition, repression of gigaxonin in zebrafish impaired motor neuron specification and somitogenesis and abolished neuromuscular junction formation and locomotion. Shh signaling was impaired in gigaxonin null zebrafish and was corrected by both pharmacological activation of the Shh pathway and human gigaxonin, pointing to an evolutionary-conserved mechanism regulating Shh signaling. Gigaxonin-dependent inhibition of Shh activation was also demonstrated in primary fibroblasts from GAN patients and in a Shh activity reporter line depleted in gigaxonin. Our findings establish gigaxonin as a key E3 ligase that positively controls the initiation of Shh transduction, reveal the causal role of Shh dysfunction in motor deficits, thus highlighting the developmental origin of GAN.

Keywords: Sonic Hedgehog signaling, Ptch receptor, gigaxonin, giant axonal neuropathy, zebrafish model, neurodevelopment, cell specification, motor neuron, neurodegenerative disease.

## INTRODUCTION

The concept of developmental defects in neurodegenerative diseases is well established for early-onset conditions, and is now emerging for late-onset pathologies where symptoms only become detectable in adulthood. Diseases presenting with cortical malformations, such as infantile epilepsy, Rett syndrome, mental retardation and autism are all considered developmental diseases. Indeed, the corresponding genes have been shown to control critical functions for neuronal development, encompassing neuronal patterning, proliferation, migration and synaptogenesis. For adult pathologies, such as Alzheimer's (AD) and Huntington's (HD) diseases, the hypothesis of a developmental signature has been supported by experimental and clinical studies, revealing the expression of β-amyloid precursor protein (APP) and Huntingtin (Htt) genes (1-3) respectively during developmental stages, and alterations of the cortex morphology in pre-symptomatic AD and HD patients using magnetic resonance imaging (4, 5). Growing evidence shows that genes mutated in late-onset diseases play essential roles during development, such as cortical progenitor migration for APP and axonal transport for Htt (6, 7). Furthermore, studies on mouse models reveal various alterations of neurodevelopmental processes: altered morphology of cranial nerves and truncated lumbar spinal nerves in Spinal Muscular Atrophy embryos (8); impairment of striatal neuron specification and maturation (9), and alteration of cortical progenitor cell division and neurogenesis (10) in HD embryos. This culminated with the direct demonstration of the implication of neurodevelopmental deficits in HD pathogenesis, in a study where mice expressing mutant Htt solely during development recapitulate the human disease (11) from the striatal neurodegeneration to the electrophysiological and motor performance deficits.

Considering that late-onset pathologies can have an origin during development, it would be reasonable to hypothesize that this is also the case for early-onset diseases. Among those, the infantile and fatal neurodegenerative disease giant axonal neuropathy (GAN) (12) represents a

strong candidate. Around 2 years of age, children experience gait difficulties accompanied by frequent falls, and become rapidly challenged in both motor a sensory modalities (13, 14). From an initial decrease of deep tendon reflexes, areflexia and amyotrophy, patients rapidly evolve towards a total loss of the deep and superficial sensitivity and of ambulation, and become wheelchair-bound during adolescence. The dramatic deterioration of the peripheral nervous system subsequently spreads to the central nervous system (CNS), causing numerous symptoms encompassing ataxia, dysarthria, nystagmus, vision impairment, intellectual disabilities and epilepsy in young adults. Altogether, the sum of symptoms leading to the death of patients in the third decade of life is incredibly extensive, and distinguishes GAN from other neurodegenerative disorders, for which a regionalization of neuronal deficits and neurodegeneration is observed. Altogether, one can presume a fundamental role of gigaxonin (15), the defective protein in GAN, in controlling a general pathway to sustain neuronal function. It is noteworthy that brain MRI of patients has revealed atrophy of the spinal cord, cerebellum and the brain stem, which would favor a global defect in brain development over a progressive neurodegeneration (16). In line with this hypothesis, a morphological marker of developmental deficit (*cavum septi pellucidi*) has been evidenced in numerous GAN patients (16). Finally, while gigaxonin expression pattern has been shown to be ubiquitously expressed, it was found to be enriched in the nervous system, and during prenatal stages (17), which may suggest a role during embryogenesis.

Our understanding of the general mode of action of gigaxonin emerges from its domain characterization as a BTB-Kelch protein (15) and its identification as an adaptor of Cul3-E3 ubiquitin ligase complex (18). In disease, the discovery that GAN mutations, which are scattered along the entire *GAN* gene confer a general instability of either the mRNA or the protein (19), supports a loss-of-function of the gigaxonin-E3 ligase activity in patients. So far, the most established substrates of gigaxonin are the Intermediate Filament (IF) cytoskeletal proteins (20), due to the fact that they represent a hallmark of the disease and can be easily investigated in

patient skin-derived fibroblasts. Thus, the broad aggregation of IFs in neuronal (Neurofilaments) and non-neuronal tissues in patients (21) has been studied in patient-derived fibroblasts, GAN mice (17, 22) and their derived neuronal models (23). According to its putative role as E3 ligase adaptor, gigaxonin imbalance was shown to either induce a dramatic clearance of multiple IF types upon excess (23, 24), or an abnormal aggregation upon depletion (25-27). The study of GAN neuronal model also unveiled the fundamental role of gigaxonin in controlling the autophagy pathway, by regulating the production of autophagosomes through the ubiquitin-dependent degradation of the ATG16L1 protein (28). While both Neurofilaments and the ATG16L1 autophagy protein have been identified as targets of gigaxonin, their respective contribution(s) to neuronal impairment and neurodegeneration in GAN remain(s) to be determined. In this context, revealing the molecular mechanisms controlled by gigaxonin is crucial.

Presently, our knowledge on the GAN pathogenesis is poor, and was mostly hampered by our inability to reproduce the severity of symptoms in the mouse (17, 22). In the present study, we generated a robust animal model of GAN in zebrafish, exhibiting the severity and penetrance of the motor deficits seen in patients. Furthermore, we combined its physiological analysis with biochemical data and studies on patient-derived cellular models to identify a substantial developmental signature in the pathogenesis of GAN, which originates from the control of Sonic Hedgehog (Shh) induction by the gigaxonin-E3 ligase.

The Hedgehog family of morphogens represents an evolutionarily conserved pathway essential for embryonic development, tissue homeostasis and tumorigenesis (29). In vertebrates, Sonic Hedgehog (Shh) assigns neuronal and muscle fate, acting in a graded manner to pattern the dorso-ventral axis of the neural tube (30) and the muscles (31). Dysregulation of the Shh cascade causes a wide range of human diseases, including congenital malformations of the CNS, of the axial skeleton and limbs, cancers and malignancies in children and adults (32, 33). The

morphogen Shh is expressed and is cleaved in the notochord and the floor plate, releasing an N-terminal active fragment, which diffuses to the receiving tissues. In progenitor cells, Shh initiates signaling by binding to the transmembrane receptor Patched (Ptch), thereby relieving the constitutive inhibition of another transmembrane protein Smoothened (Smo) and allowing its accumulation on the cell surface (34). Activated Smo transduces Shh signal by inducing the nuclear translocation and the activation of Ci/Gli transcription factors to trigger the expression of patterning and differentiation genes. In vertebrates, the components of the Shh pathway are localized to the primary cilium of the cell, which is an essential organelle for its transduction. The disruption of ciliary components alters Shh activity (35), in a tissue-dependent manner, either promoting or inhibiting signal transduction (36, 37).

Little is known about how Shh activity is fine-tuned, but ubiquitination has emerged as an important mechanism. The degradation of Shh components by ubiquitination is key in regulating the signaling pathway. In particular, the ubiquitination of Ci/Gli and its regulatory complex has shown to play a pivotal role in providing a negative feedback loop for downstream Shh signaling (38). In the absence of the morphogen, partial degradation mediated by the Slimb/Trcp -E3 ligases converts Ci/Gli into a transcriptional repressor, while the Shh cascade is turned-off after the complete degradation of active Ci/Gli by the HIB/Spop/Itch E3 ligases (38). Ubr3-E3 ligase acts in a positive feedback loop to degrade Cos2/Kif7, a negative regulator of the Hh pathway (39), while the MIDI E3 ligase has been shown to mediate the ubiquitin-dependent cleavage of Sufu, another negative regulator of the Ci/Gli activity (40). On the other hand, the de-ubiquitinase Usp7/HAUSP positively regulates signal transduction by stabilizing Ci/Gli (41), which suggests a very balanced relationship between ubiquitination and de-ubiquitination to control Shh activity. Although the downstream Shh cascade has been well studied, less is known about how the Ptch receptor, the entry point of Shh signaling, is regulated. The Smurf-E3 ligase acts on the unbound Ptch as a mechanism to turn off Shh activity (42, 43), and the E3 ligase Itchy regulates the basal

turnover of Ptch in the absence of the morphogen, to control the non-canonical Hh signaling (44). Thus, whilst the last decade has shown that ubiquitination serves as a pivotal mechanism in regulating Shh activity, the identity of the E3 ligase(s) that controls Ptch degradation in the presence of the morphogen, necessary for the derepression of the signal transducer Smo, is unknown.

Here, we identify gigaxonin as the E3 ligase controlling the initial steps of Shh induction, which is sufficient to specify neuronal and muscle fate in vertebrates. Using the zebrafish as a model system, we provide physiological evidence to show that the gigaxonin-E3 ligase is a key regulator of Shh activation, by controlling the degradation of the Ptch receptor in a Shh-dependent manner. Both transient and genetic repression of gigaxonin impairs spinal motor neuron specification and abolishes motility in zebrafish. The deficits of the gigaxonin-null embryos reproduce numerous animal models of Shh inhibition, and are restored upon Shh activation. The positive control of gigaxonin on the pathway is Shh-dependent, as revealed independently in the gigaxonin-depleted zebrafish, in a cellular system using a Shh activity reporter assay, and in human patient cells. Furthermore, gigaxonin interacts with Ptch and mediates its degradation in a Shh-dependent manner, hence identifying gigaxonin as key regulator of the initiation of Shh signaling. Notably, our findings obtained in the GAN zebrafish model mimic the motor dysfunctions found in patients, hence providing the first hints, to our knowledge into the pathophysiological mechanisms in GAN, and supporting a developmental origin in the pathogenesis of GAN. This notion is further endorsed by the functional rescue of the developmental deficits in the *gan* zebrafish by the human gigaxonin, and the evidence of an impairment of Shh signaling in patient cells.

## RESULTS

### Identification and expression pattern of gigaxonin in zebrafish

In the present study, we identified a unique gigaxonin orthologue in zebrafish by bioinformatic analysis. Extension of the partial coding sequences from the zebrafish (XM003200434, AL923051 and GO940773) allowed us to clone the full-length *gan* cDNA (released to Genbank and zebrafish databases, BankIt1829960, zebrafish KT013299, respectively). Similar to humans, the zebrafish *gan* gene is composed of 11 exons and encodes for a protein of 609 amino acids with a N-terminal BTB domain and a 6 kelch repeat domain in its C-terminal part (Figure S1). Zebrafish gigaxonin (z-gigaxonin) is closely related to its mammalian homologues and exhibits a high degree of conservation with the human protein (78 % identities and 80 % similarities) (Figure S1).

To determine the expression pattern of z-gigaxonin, we combined whole-mount in situ hybridization with RT-PCR experiments. Analysis of *gan* transcripts revealed ubiquitous and constant expression from early embryogenesis through juvenile/adult stages (Figure S2A and 2C, left panel), with enrichment in the eyes, the notochord, the muscles and the heart. (Figure S2A). Interestingly, the detection of *gan* mRNA at the zygote stage demonstrates that maternal transcripts are present in the embryos, before the midblastula transition.

### Gigaxonin depletion causes severe morphological abnormalities

To investigate the function of gigaxonin in zebrafish development, we first took a transient repression approach to enable a dose-response analysis. Indeed, we intended to achieve a significant decrease of z-gigaxonin abundance, without totally abolishing it, to more closely mimic the spectrum of GAN mutations in patients, for which a general mechanism of instability was demonstrated (19). Thus, we impaired *gan* pre-mRNA splicing with anti-sense morpholino oligonucleotide (MO), at the acceptor splice site of exon 3 (Figure S2B). The effective disruption of splicing was confirmed by RT-PCR in morpholino-injected embryos (called *gan* morphants)

from 10hpf and from a dose of 0.25 pmol of *gan* oligonucleotides (Figure S2C, right panel). Importantly, increasing doses of morpholino were compared to identify 0.25 pmol as a non-toxic dose that did not perturb the global development and the number of somites at 24hpf, as compared to non-injected embryos (Figure S2D).

Injection of *gan* morpholino, and not the 5-bp mismatch control morpholino induced significant abnormalities from 48 hpf, as revealed by hematoxylin/eosin staining of whole embryos (Figure S3A). Morphants exhibited penetrant and strong morphological phenotypes, including shortened body length, absent yolk extension, pronounced head and eye atrophies and heart defect (Figure S3B). Importantly, the developmental deficits of *gan* morphants were rescued by co-injection of human *GAN* mRNA, hence confirming the specificity of the morpholino and the functional conservation of gigaxonin between zebrafish and human (Figure S4A). Additionally, we disrupted *gan* mRNA processing with another MO, targeting the acceptor splice site of exon 2 (MO ex1-2), and obtained similar morphological deficits (data not shown).

**Gigaxonin depletion impairs motility in zebrafish**

In regards to the neuronal and muscle expression of gigaxonin during development, we investigated the motor performances of the *gan* morphants, upon touch stimulation and during spontaneous motility. The analysis revealed a marked reduction of motility in gigaxonin-depleted animals. The touch-response assay, performed at 72hpf, revealed swimming abnormalities in 72.4 % of the morphants, with a circular swim (referred to as *looping*), circular swim around the axis of the head (referred to as *pinwheel)* or absence of motion (referred to as *motionless*) (Figure 1A, B and movie 1).

To confirm these results and evaluate pure motor capacities, we monitored the spontaneous locomotion of 5dpf old larvae. The spontaneous motility of *gan* morphants was considerably impaired. While 80% of the morphants did not move, the remaining moved significantly slower and over a shorter period than control larvae (Figure 1C and 1D). The specificity of the motility

defects for gigaxonin was demonstrated by the rescue upon co-injection of human *GAN* mRNA (Figure S4B).

**Gigaxonin is required for the specification of secondary motor neuron**

To explore the role of gigaxonin in sustaining motility in zebrafish, we analyzed the two consecutive waves of motor neuron birth in the spinal cord: the primary Motor Neurons (pMN) and secondary Motor Neurons (sMN), born between 9-16 hpf and 14-51 hpf respectively (45). Analysis of different key developmental stages using the islet marker revealed a normal proportion of pMN at 20hpf (Figure S5A), but a substantial reduction of sMN at 36hpf in morphants compared with the control group (Figure 2A). The similarities with zebrafish carrying mutations in the Shh pathway (46-48) prompted us to test whether the decrease in MN number might result from an impaired cell specification in the *gan* morphants. For that purpose, we labeled MN progenitors with the Shh target gene *Nkx6.1*. While the number of Nkx6.1 positive progenitor cells was not notably affected in morphants at 20hpf (Figure S5A), Nkx6.1 expression was markedly reduced prior to sMN differentiation from 28hpf onwards (Figure S5B, C).

These data indicate that gigaxonin depletion inhibits sMN specification through a decrease of Nkx6.1 expression in progenitor cells, as would do an inhibition of Shh signaling during the second wave of MN birth. As a result, the structure of the spinal cord was severely impaired in older embryos, with decreased motor neurons as revealed by ultrastructural examination at 72hpf (Figure S6A). We found this effect of gigaxonin to be specific to spinal motor neuron specification, as the Islet positive branchiomotor neurons in the hindbrain were not affected in *gan* morphants at 48hpf (data not shown).

Collectively, our data demonstrate a role of gigaxonin in controlling the differentiation of secondary motor neurons in the zebrafish spinal cord.

**Gigaxonin controls the axonal pathfinding of primary motor neurons**

The absence of sMN in *gan* morphants was further confirmed by immunostaining using the specific neuronal cell surface marker Zn8. Indeed, Zn8 positive cells were completely absent in morphants at 56hpf (Figure 2B), when sMN axonogenesis in control embryos is finished. Next, we determined whether gigaxonin-depleted pMN exhibit any defects in axonal pathfinding. At 56hpf, repression of gigaxonin resulted in a wide range of axonal defects. Concomitant to an increased arborization of primary motor axons, *gan* morphants exhibited an aberrant growth of pMN axons reminiscent of Shh mutants (46), including an absence or significant shortening of the caudal (CaP) primary axons (Figure 2C-E) and misguided axons with ectopic ventral projections. Interestingly, the three-dimensional view of 48hpf morphants indicated additional phenotypes (Figure 2D, left panel and associated movies 2 and 3). Indeed, morphants exhibited abnormal protrusions of axons from the spinal cord, and an apparent absence of the MiP and RoP motor axons, leading to an overall profound alteration of the structure of the spinal tracts and an increased spacing between the two motor columns.

Importantly, the axonal deficits and the absence of sMN were reproduced by targeting an independent region of the zebrafish *gan* mRNA (MO ex1-2) (Figure S7A), and rescued upon co-injection of human *GAN* mRNA (Figure S4C), hence demonstrating the specificity of gigaxonin depletion.

**Gigaxonin promotes muscle innervation and somitogenesis**

The severity of the defects in both pMN and sMN, together with the locomotion disabilities in morphants prompted us to investigate the integrity of the neuro-muscular junction and muscles. Visualization of acetylcholine receptors using α-bungarotoxin staining revealed a total absence of synapses along the axons at 48hpf, as compared to control embryos (Figure 2D, movies 2 and 3). We further analyzed the muscle integrity to reveal profound structural abnormalities of muscles trunk somites in *gan* morphants at 48hpf. Unlike control zebrafish, which have V-shaped somites and well-organized myofibers, *gan* morphants exhibit U-shaped somites with an absence of

horizontal myoseptum, and less dense and wavy myofibers (Figure S6B). Similar to Shh inactivation (46, 48), this effect was further reproduced using MO ex1-2 for *gan* (Figure S7B) and was detected as early as 28hpf, concomitantly to the abnormalities of pMN axonal pathfinding (data not shown), which may suggest a dual effect of gigaxonin in neuronal and muscle development. Ultrastructural examination of morphant muscles at a later stage further revealed a substantial alteration of myofiber structure, characterized by a marked shrinking of myofibers, an apparent denser content and an invasion of conjunctive tissue (Figure S6C). While control embryos presented a regular hexagonal arrangement of the thick filaments with intercalating thin filaments (Figure S6C), morphants exhibited a disorganization of sarcomeres, with a pronounced disparity in the spacing and distribution of the myosin and actin filaments.

**_Gan_ deletion zebrafish mutant recapitulates the _gan_ morphant phenotype**

To confirm the specificity of our Shh-like phenotypes for gigaxonin, we generated a *gan* knock-out zebrafish line ($gan^{del/del}$), by deleting the entire endogenous gene (Figure 3A). Interestingly, large mutations have been evidenced in GAN patients (19, 49). Similarly to the *gan* morphants, we found that $gan^{del/del}$ zebrafish display normal morphology at early stages of development, but present with severe locomotor impairments. Using a touch-response assay at 72hpf, we identified 49.1% of $gan^{del/del}$ zebrafish with swimming defects, among which 76 % of $gan^{del/del}$ zebrafish were unable to move (Figure 3B). The impairment of motor function was directly confirmed at 5dpf, when 80% of the total mutants exhibited severe defects in spontaneous locomotion assay, with a significant reduction in both total distance and net velocity (Figure 3C, D).

We then examined the specification of sMN by labeling MN progenitors with the transcription factor *Nkx6.1*. As observed in morphants, the number of Nkx6.1 positive cells was dramatically decreased in 85% of $gan^{del/del}$ mutants at 36hpf (Figure 3E). No significant change was found in the number of MN progenitors cells at earlier developmental stages, between 20-28 hpf (Figure S5).

At 56hpf, *gan* deletion resulted in a substantial reduction in the number of sMN and an aberrant growth of their axons, as labeled with the markers Islet and Zn8 respectively (Figure 3F). This axonal phenotype occurred in 72% of *gan*$^{del/del}$ zebrafish.

Altogether, the similarity of the phenotypes between the *gan* genetic mutants and the transiently inactivated z-gigaxonin animals demonstrate that the neurodevelopmental deficits observed in this study are specifically controlled by the gigaxonin encoding gene.

**Shh activation restores neuronal specification and somitogenesis deficits in gigaxonin-depleted zebrafish**

Shh signaling is crucial for the specification of neuronal identity and for somitogenesis. Genetic and pharmacological ablation of Shh pathway in zebrafish have been shown to abolish motor neuron specification in the spinal cord and to generate U-shaped somites (42, 45, 47, 48, 50). The striking similarities with our morphants indicate a potential role of gigaxonin in regulating Shh activity in zebrafish. A first validation towards a downregulation of the Shh pathway in GAN was provided by the pronounced reduction in the expression of the Shh responsive target *Nkx6.*1 gene in the spinal cord of *gan* morphants (Figure 2A). To further expand on these results, we modulated Shh signaling in zebrafish, to either inhibit or activate it, using cyclopamine and purmorphamine respectively. We demonstrated that cyclopamine administration during the second wave of MN birth (from 14hpf to 48hpf) in wild-type embryos fully reproduces the phenotype induced by gigaxonin depletion. Treated wild-type embryos exhibited both an aberrant somitogenesis with U-shaped structures (Figure 4A) and a total loss of sMN (Figure 4B), while 80% of the embryos also displayed *pinwheel* swimming behavior upon mechanical stimulation at 72hpf (data not shown). Conversely, the elevation of Shh signaling in *gan* morphants (by purmorphamine) suppressed the muscle deficits, as shown by the restoration of V-shape somites and denser myofibers (Figure 4A). The restoration of MN differentiation was not so robust when the drug was administered during sMN specification, as revealed by the partial rescue of Zn8

staining in *gan* morphants (Figure 4B). Remarkably, the restoration of sMN differentiation in morphants was more efficient when purmorphamine was applied earlier, from the first wave of MN birth (8hpf-48hpf) (Figure 4C), indicating a possible control of the Shh cascade by gigaxonin from 8hpf. While these results could suggest that Shh activation is beneficial to GAN independently of gigaxonin's mode of action, the decreased expression of the Shh target *Nkx6.1* gene in morphants, together with the similarities between our and numerous Shh defective models, rather indicate that gigaxonin functions as a positive modulator of the Shh pathway in zebrafish, to promote both neuronal and muscle development.

**Gigaxonin acts as a positive regulator of the Shh signaling**

To directly demonstrate that gigaxonin acts on the Shh pathway, we studied its activity in three independent biological systems where gigaxonin expression was ablated. Firstly, we performed in situ hybridization on the *gan* morphants and the *gan*$^{del/del}$ line to assess the expression pattern of *ptch2*, a direct target of Shh signal transduction and a well-established indicator of Shh activation (Figure 5A). In the spinal cords of zebrafish embryos at 32hpf, *ptch2* displayed a ventral-high dorsal-low pattern of expression. In conditions where gigaxonin expression was reduced, either through MO knock-down or genetic ablation, the expression of *ptch2* in the spinal cord was dramatically decreased (Figure 5A), hence evidencing an inhibition of Shh signaling in the absence of gigaxonin. Secondly, we knocked down gigaxonin with RNAi in Shh-Light2 cells (Figure 5B, left panel), an NIH-3T3 cell line that is stably expressing a Gli-dependent luciferase reporter and becomes activated upon Shh stimulation (51). In this study, we demonstrated that while Shh alone increased the activity of the luciferase 19-fold, the decrease in gigaxonin levels diminished this effect by 22% (Figure 5B, right panel). Importantly, this effect was only significant in the presence of the morphogen, and not under basal conditions, which indicates an effect specifically upon Shh activation. Thirdly, we analyzed primary fibroblasts derived from GAN patients, which represent a well-established cellular model for the human pathology (25,

26). We selected independent primary fibroblasts carrying different mutation types representative of the pathology: large deletion ($GAN^{\Delta ex10\text{-}11}$) and a missense mutation ($GAN^{A49E}$) for which gigaxonin was dramatically reduced (19). Conveniently, human primary fibroblasts present primary cilium, the antenna for Shh signaling in vertebrates, which can be easily detected. An established and well-documented method to identify Shh activation is the detection of the translocation of Smo into the cilium in the presence of the morphogen (52). Here we showed that while in the control human fibroblasts exposed to Shh-CM for 4h Smo localization to the cilium was significantly increased, this action was dramatically reduced in GAN patient primary fibroblasts (Figure 6A). Not only does the Shh pathway rely on the presence of cilium for signal transduction, but intraflagellar transport particles of the cilium and downstream targets of Shh have also been shown to regulate cilium length to modulate Shh signaling (35). Thus, as a second readout for Shh responsiveness, we compared the cilium length between control and mutant primary fibroblasts upon Shh induction. Interestingly, whilst the control human fibroblasts exposed to Shh increased the cilia length by 29% (Figure 6B), the ciliary length of the independent GAN fibroblasts was not altered upon Shh addition, hence showing their inability to respond to the Shh activation. Altogether, we demonstrate here that Shh fails to activate properly in the absence of gigaxonin in zebrafish, mouse and human systems, hence providing substantial evidence for the critical role of gigaxonin in promoting Shh induction.

**Gigaxonin acts together with Shh to degrade the receptor Ptch and initiate the signaling cascade**

To gain an insight into the molecular mechanism by which the gigaxonin-E3 ligase positively controls the Shh signaling, we directly addressed whether gigaxonin can act together with Shh to target Ptch for degradation, and therefore initiate the Shh pathway. Using both loss- and gain-of-function methodologies, we investigated the levels of endogenous Ptch in the presence or absence of Shh. Overexpressing gigaxonin, with or without Shh, provided evidence that endogenous Ptch

could only be efficiently degraded when both gigaxonin and Shh were added to the system (Figure 7A). Conversely, reduction of the levels of endogenous gigaxonin with RNA interference revealed an increase in the abundance of endogenous Ptch, which was exacerbated when Shh was present (Figure 7B). From these results, we hypothesized that gigaxonin might interact with Ptch. Indeed, using a co-immunoprecipitation (co-IP) assay in Light2 cells, we detected the presence of endogenous Ptch in the gigaxonin complex (Figure 7C). We confirmed these results by overexpressing both Cherry-Ptch and Flag-Gig in COS cells and performing co-IP in both directions (Figure 7D). Interestingly, we observed multiple bands with Cherry-Ptch in gigaxonin immunocomplex, resembling the laddering characteristic of ubiquitination. We confirmed this by co-labeling the Cherry-Ptch signal with anti-Ubiquitin antibody exhibiting specific Lysine-48 linkage antibody, hence identifying poly-ubiquitinated Ptch in gigaxonin complex. The comparison with Ptch immunocomplex was also informative. Beyond the confirmation of the interaction of both proteins, the absence of laddering of Ptch and the weaker pull down of gigaxonin revealed that while gigaxonin does not interact with the entire pool of Ptch within the cell, the gigaxonin complex is significantly enriched in ubiquitinated Ptch. Collectively, our data demonstrate that gigaxonin acts positively on the Shh pathway, through the interaction with the Ptch receptor and a Shh-dependent targeting for degradation.

## DISCUSSION

In this study, we combined physiological evidence, cellular assays and biochemical data to discover a causal role of developmental dysfunctions in the pathogenesis of GAN in the motor system, whereby gigaxonin-E3 ligase loss-of-function inhibits the Shh pathway. Controlling the degradation of the Ptch receptor, the upstream components of the cascade, and in a Shh-dependent manner, we propose gigaxonin-E3 ligase as a key molecular switch for the initiation of the signal transduction mediated by Shh (Figure 7E). Examined at an organism level in zebrafish, this gigaxonin-mediated regulatory mechanism is essential for specifying both neuronal and muscle patterning to sustain locomotor activity in vivo, and its perturbation mirrors the loss of ambulation seen in GAN patients. Notably, the ability of the human gigaxonin to fully rescue the deficits in the *gan* zebrafish model, combined with the evidence of an impairment of Shh signaling in patient cells, support a functional conservation of this developmental signature in patients.

Here, we provide conclusive evidence of the physiological role of gigaxonin in positively regulating the Shh pathway in vivo. Firstly, we show that gigaxonin depletion mimics the loss-of-Shh phenotype. Both MN specification and somitogenesis are compromised in *gan* morphants, causing sMN loss and U-shape somites similarly to the pharmacological and genetic inhibition of the Shh pathway through loss-of-function of Smo (46, 48), Gli (47, 50) or Shh (53). Secondly, we show that the absence of sMN results from the impairment in the differentiation of progenitor cells, as evidenced by the downregulation of the Shh-responsive *Nkx6.1* target gene from 28hpf onwards. These Shh-like phenotypes and markers were also evidenced in the CRISPR *gan* knock-out zebrafish line, which demonstrates the specificity of the phenotypes towards gigaxonin functions. Thirdly, in situ hybridization in both *gan* morphants and $gan^{del/del}$ line revealed a reduced expression of *ptch2*, the target of Shh cascade, hence directly demonstrating the inactivation of Shh signaling in zebrafish depleted in gigaxonin. Lastly, pharmacological

activation of the Shh pathway was able to restore both neuronal specification and somitogenesis in *gan* morphants, in agreement with the function of gigaxonin in positively regulating Shh activity. We further confirmed this statement in independent biological assays, using both a mouse Shh reporter cell line depleted for gigaxonin and human primary fibroblasts derived from GAN patients. Using established readouts for Shh activation, i.e. transcriptional activation (51), Smo localization to cilium (52) and cilium length (35), we demonstrated in both cellular systems an impairment of gigaxonin-depleted cells to respond to Shh induction.

Amongst other morphogenic pathways (Wnt, BMP, FGF…), Hedgehog is unique as it relies on a paucity of activating ligands and on a single downstream signaling cascade, hence placing gigaxonin as a key molecular determinant to decipher its physiological regulation, necessary to ensure spatio-temporal and process specificity. In this study, we add insights into the regulation of the Shh pathway in the context of the motor system. Our investigation of MN birth, which occurs in two sequential waves in zebrafish (9-16hpf for pMN and 14-51hpf for sMN) (45) revealed a specific impairment of sMN specification during the second wave in *gan* morphants. In these animals, pMN specification seems correctly achieved, but severe defects were observed during the axogenesis process, which takes place during the first day of development. While the maternal *gan* mRNA (as shown in Figure S2A) may partially compensate for Shh activation during the first wave of MN birth, our results may also suggest a differential and temporal regulation of the canonical and non-canonical roles of Shh by gigaxonin. Indeed, the misguidance of CaP pMN axons in *gan* morphants, which are comparable to Smo mutants (46), may be caused by the reported non-canonical functions of Shh in controlling axon guidance and axon fasciculation (54, 55). Intriguingly, our pharmacological experiment using purmorphamine revealed that the restoration of MN specification was not efficient when applied during sMN birth, but required a treatment during the first wave. These data reinforce the notion that the two critical periods of MN induction are not independent and that Shh activity in the first wave is a

key temporal determinant for the second one, as previously illustrated by the absence of sMN in embryos subjected to cyclopamine treatment for a short 4-10hpf period (46). Thus, our results reveal severe defects in pMN axonal pathfinding in morphants and may offer interesting speculations on the control of MN fate by axonal determinant.

While this study provides important insights into the control of the Shh pathway by gigaxonin within the motor system, it might also be possible to extend this to other modalities, within and outside the nervous system. Indeed, we showed that gigaxonin is enriched in the nervous system and during prenatal stages (17), but its expression is ubiquitous. Thus, one could suggest that the coexistence of Shh cascade and gigaxonin within the same tissue would provide the context specificity of this control, extending beyond the nervous system. Accordingly, Shh signaling has been implicated in the development of multiple non-neuronal tissues (29), including skin, hair, mammary gland, stomach and kidney, all of which are reported to be affected in GAN patients (13). As the substrate adaptor of an E3 ligases complex, the ubiquitous gigaxonin may also be functionally silenced in tissues insensitive to Shh, through post-translational modifications, or by limited amount of the other subunits. Thus, GAN is commonly defined as a neurodegenerative disease, due to the massive deterioration of the entire nervous system, but should be more adequately investigated beyond the nervous system, to shed light into other possible damaging phenotypes that would reflect a global impairment of Shh signaling, as extrapolated from our study.

E3 ligases and ubiquitination constitute a pivotal mechanism of Shh regulation, by providing both negative and positive feedback loops on Shh activation, and therefore playing a key role in fine-tuning Shh responses. Although it is well studied for the transcription factor Ci/Gli, little is known about the regulation of the early steps of Shh activation. Previous studies have shown that ubiquitination of the transducer Smo and the Shh-bound Ptch receptor are essential to trigger Shh activation, but the identity of the E3 ligase(s) that control the initiation of the pathway are

unknown. Here, we show that the gigaxonin-E3 ligase plays a role in the early steps of the Shh cascade, mediating the degradation of the Ptch receptor necessary to relieve the constitutive inhibition of Smo. We showed that gigaxonin interacts with endogenous Ptch and that its degradation is potentiated by the presence of Shh, hence placing gigaxonin as the first E3 ligase, to our knowledge, that enables the receiving cells to interpret the morphogen signal. Indeed, the E3 ligases Itchy and Smurf act on Ptch to control the basal turnover of the receptor in the absence of the morphogen (44), or unbound Ptch as a mechanism to turn-off Shh signaling, respectively (42).

We previously identified the gigaxonin-E3 ligase (15) and two of its targets: the IF proteins (20, 24), and the autophagy protein ATG16L1 (28). Through direct binding and ubiquitination, gigaxonin controls the steady state of these cellular compounds, to balance the homeostasis of cytoskeleton within neuronal and non-neuronal cells and regulate the autophagic flux within neurons. These studies have uncovered the crucial role of gigaxonin in fine-tuning two fundamental cellular processes, but the demonstration of their respective implication in neuronal dysfunctions in GAN has yet to be provided. The characterization of the neurodegenerative model in GAN neurons (28) will permit such investigation in the future. While we do not exclude any potential contribution of the known effectors of gigaxonin to disease, we have identified here the Shh pathway as a novel target for gigaxonin, which is sufficient to mimic the motor deficits seen in patients.

To closely mimic the genetic spectrum of mutation in GAN, we deprived the zebrafish gigaxonin, using a transient and a stable knock-out approach. Both systems revealed severe and penetrant motor deficits, with loss of locomotion in 80% of z-gigaxonin depleted animals, as a result of denervation, impaired motor neuron specification and somitogenesis, hence supporting a loss-of-function mechanism in GAN. To our knowledge, the zebrafish model we describe here represents the first and heretofore most robust animal model for GAN, given that it emulates the severity

and penetrance of the motor deficits seen in patients (13, 14). Indeed, attempts by our and other laboratories revealed only modest and late-onset sensory-motor symptoms in distinct GAN mice, with no overt neuronal damage (17, 22). Future examination of the zebrafish model in adult stage will be important, in regard to phenotype and survival. In particular, it will allow for confirmation of locomotion defects in adults, and investigation of the myriad of late-onset symptoms seen in patients, which develop in the CNS, encompassing ataxia, dysarthria, nystagmus, vision impairment, intellectual disabilities and epilepsy in young adults.

Noticeably, Shh impairment leads to a pleiotropic phenotype that sums up the variety of symptoms found in GAN patients, in the CNS and PNS. Indeed, mutations in components of the Shh pathway in human cause ataxia (56), vision impairment (57), intellectual disabilities (58) and epilepsy (59). While this has to be confirmed in the *gan* zebrafish, the similarities of symptoms between the Shh models, GAN patients and our study support a main role of Shh dysfunction as a causal mechanism in the GAN pathogenesis. This hypothesis is further sustained by i) the massive atrophy of neuronal tissues in brain MRI of patients, ii) the detection of a morphological marker of developmental deficit in patients (16), iii) and the enrichment of gigaxonin in neuronal tissues and in prenatal stage (17). Thus, further work would be important to determine whether the impairment of Shh signaling during development is sufficient to cause adult symptoms. Awaiting for this demonstration, GAN exemplifies the emerging concept whereby neurodevelopmental deficits disrupt homeostasis and generate vulnerability that further evolves towards clinical manifestations in adulthood, as shown in HD (9-11) and AD (7) diseases.

To our knowledge, this study provides the first hints for the hypothesis that the human GAN pathology has a neurodevelopmental component, but it also opens an exciting new avenue for a role of the Shh pathway in adulthood. Indeed, in the mammalian adult brain, Shh signaling has emerged as an important neuromodulator through different mechanisms, including the proliferation of postnatal neural stem cells and fate specification (60, 61). One could therefore

speculate for the human pathology, that the gigaxonin-mediated Shh repression can act at multiple levels in prenatal and postnatal stages. Since GAN is an early-onset pathology, a more comprehensive study aimed at deciphering the control of Shh signaling by gigaxonin during development and in adulthood could shed light on the possible treatment windows for this yet incurable and fatal disease. In light of the therapeutic benefits obtained by modulating the Shh pathway in several neurodegenerative conditions (60), our study may also offer a specific target for therapeutic intervention aimed at reactivating neurogenesis in disease.

## METHODS

***Genebank zebrafish** gan **cDNA accession number.*** The full zebrafish *gan* cDNA was sequenced and released in Genebank database under # KT013299; the corresponding gigaxonin protein ID is # ANJ65950.

***Animals and Morpholino knock-down.*** Zebrafish (*Danio rerio,* Oregon AB) were maintained at 28.5 °C and on a 14:10 h light:dark cycle and staged by hours (h) or days (d) post fertilization. The *gan* antisense Morpholino Oligonucleotides (MOs, Gene Tools) and mismatch Morpholino (Mis) were microinjected into one- to two-cell stage embryos according to standard protocols. 1nl volume was injected at a concentration of 0.25 mM for the MO/Mis ex2-3 and 0.6 mM for the MO ex1-2 (sequences in Table 1).

***rtPCR.*** mRNA extraction was performed on dechorionated embryos at specific times using Trizol (Sigma-Aldrich). cDNA was obtained after reverse transcription (SuperScript III Kit, Invitrogen) and *gan* coding sequences were obtained with the primers *gan* exons 2-3 and *gan* exons 3-4, as presented in Table1.

***Generation of the CRISPR gan zebrafish*.** The $gan^{del/del}$ zebrafish line was generated using the genome-editing technology CRISPR (AMAGEN, Gif-sur-Yvette, France). Six distinct guide RNAs were selected against off-target, using the CRISPOR tool (http://crispor.org; (62)) and designed within exon 1 and exon 11 of the zebrafish *gan* gene. They were co-injected with Cas9 protein into zebrafish eggs, and their efficacy and toxicity were compared at 48hpf. The selected sgRNA were used to create the $gan^{del/+}$ line, whose deletion lies between the middle of exon 1 and downstream of the stop codon in exon 11. As confirmed by sequencing, the resulting Open Reading Frame is restricted in exon 1 and contains several premature STOP codons, with only 43 amino acids produced. F3 Transgenic *gan* zebrafish were crossed to obtain fertilized $gan^{del/del}$ eggs, with an average of 10% lethality. Genotyping was performed as following: genomic DNA

extraction was performed by collecting tail pieces from anesthetized embryos into lysis buffer (10mM Tris-HCl pH8, 2mM EDTA pH8, 0.2% Triton 100X, proteinase K) boiled for 10' at 96°C. Genomic DNA containing deleted sites was PCR-amplified using primer sequences presented in Table 1 and separated on a 2% agarose gel.

***(Immuno)histochemistry and electron microscopy of zebrafish embryos.*** Zebrafish were treated with 75µM PTU from 10hpf to prevent pigmentation. At appropriate developmental stages, they were anesthetized with 0,0168% tricaine (MS-222, E1052, Sigma-Aldrich), and fixed in 4% PFA for 4h at RT or overnight at 4°C, and permeabilized in 1X PBS-1%TritonX-100 for 2h on an orbital shaker. The embryos were incubated in blocking buffer (1%DMSO, 1% normal donkey serum, 1% BSA, 0.7% TritonX-100, PBS) for 1h at RT and incubated in primary antibodies overnight at 4°C. Primary antibodies were from following sources: mouse IgG2b anti-islet 1/2 (1:100, 39.4D5, DSHB), mouse IgG2a anti-synaptotagmin 2 (1:100, Znp-1, DSHB), mouse IgG1 anti-neurolin (1:100, Zn8, DSHB), mouse IgG1 anti-Nkx6.1 (1:20, F55A10, DSHB), mouse IgG1 anti-dystrophin (1:20, MANDRA1 7A10, DSHB), rabbit anti-smoothened (1:150, Ab38686, Abcam), mouse IgG2a anti-Arl13b (1:150, N295B/66, NeuroMab), anti-α-bungarotoxin Alexa Fluor™ 555 conjugate (1:50, B35451, Invitrogen). Following 0.1% TritonX-100:PBS washes, the embryos were incubated in secondary antibodies overnight at 4°C. For immunofluorescence, Alexa Fluor™ 488, Alexa Fluor™ 594 and Alexa Fluor™ 647-conjugated secondary antibodies were from Jackson Labs (1:500, 200-542-211, 200-582-211 and 200-602-211 respectively). Imaging was performed using confocal laser scanning microscope model LSM700 (Carl Zeiss). Quantification of projection lengths was obtained with ImageJ software and 3D acquisitions were performed with LightSheet Z.1 microscope (Carl Zeiss). For Hematoxylin/Eosin contrast, the embryos were fixed in 4%PFA:PBS for 2h at RT followed by permeabilization in PBS-1% Triton X-100 for 2h. After washes in ethanol, the embryos were incubated for 2min in 0,1% Eosin, washed in ethanol and incubated in 1:10 Hematoxylin for 40sec. Bright field images were taken

on a SPOT camera mounted on a Zeiss Axioplan 2 imaging microscope. TEM analysis has been performed in 72hpf larvae, using protocol described in (63).

***Locomotion assays.*** The touch-response test was performed on 72hpf larvae, by a slight mechanical stimulation. The motion of individual larva was examined and scored as « normal swimming », « looping swimming », « pinwheel swimming », or « motionless ». Representative tracking from movies were obtained with the ImageJ software. The spontaneous motility of zebrafish were monitored at 5dpf, using the Zebrabox recording system (Viewpoint). The tracking of the motility was recorded for individual zebrafish on a 96-well plate for 1 hour, and presented as slow (3-6mm/s) and high velocities (>6mm/s).

***Pharmacological modulation of Shh pathway in zebrafish.*** In vivo inhibition and activation of Shh signaling was achieved with incubation of dechorionated embryos in 50µM cyclopamine hydrate (C4116, Sigma-Aldrich) and purmorphamine (SML0868, Sigma-Aldrich), respectively. Analysis of embryos was performed at 48hpf, after a treatment window targeting the birth of both primary and secondary motor neurons (from 8hpf) or uniquely the secondary wave (from 14hpf).

***Cloning of early players of the Sonic hedgehog pathway in zebrafish.*** Zebrafish mRNAs were extracted using Trizol (Sigma-Aldrich), and subjected to reverse transcription (SuperScript III Kit, Invitrogen). cDNAs of Ptch1 and gigaxonin were amplified by PCR using primers flanked with ATTB1/ATTB2 sequences and cloned in the pcDNA-mCherry-N and pCi-3xFlag-N gateways vectors, respectively. Gigaxonin cDNA was cloned from (25) in the pcDNA-mCherry-N gateway vector. See Table 1 for the sequences of primers.

***Cell culture.*** NIH-3T3 cells (ATTC clone CRL-1658) were grown in DMEM supplemented with 10% NBCS, 1% Pen, 1% Strep. Light-2 cells (provided by P. Beachy, GRCF Biorepository & Cell Center, Johns Hopkins, USA) were cultured in DMEM supplemented with 10% FBS, 0.4mg/ml G418, 0.15mg/ml Zeocin (51). COS-7 cells (ATTC clone CRL-1651) were grown in

DMEM supplemented with 10% FBS, 1% Pen 1% Strep. Transfection with pci 3xFlag-Gig, pcDNA-mCherry-Ptch/Gig plasmids was performed using Lipofectamine 2000 (Thermo Fisher Scientific). 24 hours after transfection, NIH-3T3 cells were treated with 3µg/ml ShhN (1314-SH, R&D Systems) (39) and Light2 cells with Shh conditioned medium (Shh-CM) obtained from ShhN expressing HEK293 cells for 48 hours (provided by P. Beachy, GRCF Biorepository & Cell Center, Johns Hopkins, USA) (64). *GAN* and mismatch siRNA were transfected using DharmaFECT 1 Transfection Reagent (see table 1 for sequences). Human control and GAN patient fibroblasts (carrying different homozygous mutation types: large deletion ($GAN^{\Delta ex10\text{-}11}$) and a missense mutation ($GAN^{A49E}$) (19, 25, 26) were grown in DMEM supplemented with 10% FBS, 1% Pen, 1% Strep. For the ciliary staining, the cells were plated on glass coverslips overnight, serum starved in 0.5% FBS for 24h and supplemented with Shh-CM for 4 or 24h as indicated.

***Biochemistry.*** At 48h or 72h post transfection, lysis of cells and immunoblotting were performed as described in (26). Briefly, the cells were incubated in lysis buffer (50mM Tris pH 7.5, 150mM NaCl, 1% Triton X-100, 5mM EDTA, and a cocktail of protease inhibitors) for 30 minutes and the supernatant retrieved by centrifugation. The proteins were separated on 8 or 10% SDS-polyacrylamide gel, transferred onto nitrocellulose membranes and blocked for 1h at RT in blocking buffer (5% milk, 0.05% Tween20, PBS). Primary antibody incubation was done overnight at 4°C, followed by PBST (0.05% Tween20, PBS) washes and secondary antibody incubation for 1h at RT. For the immunoblotting, primary antibodies were from the following sources: mouse anti-GAPDH (1:2000, AM4300, Ambion), mouse anti-tubulin alpha (DM1α) (1:1000, CP06, Calbiochem), mouse anti-Flag (M2) (1:2000, F3165, Sigma-Aldrich), mouse anti-mCherry (1C51) (1:2000, Ab125096, Abcam), rabbit anti-Patched1 (1:100, Ab53715, Abcam), rabbit anti-Ubiquitin, Lys48-specific (K48) (1:1000, 05-1307, Millipore). HRP-secondary antibodies were from the following sources: goat anti-rabbit (1:5000, 31460, Millipore), goat

anti-mouse (1:5000, 31430, Millipore), rat anti-mouse IgG (1:1000, ab131368, Abcam). Fluorescent-labeled secondary antibodies used for immunoblotting were: donkey anti-mouse IRDye 800 CW (1:15000, #926–32212, Eurobio), donkey anti-rabbit IRDye 680 RD (1:15000, #926–68073, Eurobio). Fluorescent and HRP secondary antibodies were revealed using Odyssey Clx (LI-COR) and ChemiDoc XRS+ (BIO-RAD) imagers respectively. In Co-IP assay, the cells were treated with MG-132 12h prior to cell lysis, and the immunocomplexes were recovered with Dynabeads® Protein G (Invitrogen) linked to specific or control mouse IgG (Santa Cruz Sc2025) antibodies, after incubation with the cell lysates. For immunofluorescence staining, the cells were plated on 12mm circular coverslips and fixed in 4% PFA for 20 min at RT. Cells were blocked for 1h at RT in blocking solution (4% BSA, 4% donkey serum, 0.1% Triton-X 100, PBS) and stained overnight at 4°C in primary antibodies. After washes in PBS, the cells were stained with appropriate secondary antibodies for 1h at RT, followed by staining with DAPI for 5 min (25). Fluorescent images were taken with a confocal laser scanning microscope model LSM700 (Carl Zeiss).

***Dual Luciferase Reporter Assay.*** The dual luciferase reporter assay was performed as previously described (64). Briefly, Shh-Light2 cells were seeded into 24-well plates the night before transfection. The cells were transfected with *GAN* or mismatch siRNA (Dharmacon) using DharmaFECT 1 transfection reagent (Dharmacon). At 24 hours post transfection, the cells were switched to low serum (2% FBS) medium and treated with conditioned medium from ShhN expressing cells as indicated. At 72 hours post transfection, the cells were lysed and luciferase activity was analysed on CLARIOstar (BMG Labtech) using Dual-Luciferase® Reporter Assay System (Promega).

***Statistics.*** The statistical significance of the differences between experimental groups was determined by the GraphPad Prism software, except for the comparison of proportions, which was realized by the R software. The assessment of the normality of the distribution of the data

was determined with the Shapiro-Wilk test, to apply either a parametric or non-parametric test. Accordingly, the parametric One-way ANOVA test (with the Bonferroni post-hoc test) was applied for Fig 2E, Fig 5B, Fig 6B, Fig S3 (lower panels); the non-parametric Mann Whitney test is applied for Fig 3D; the non-parametric Krustal-Wallis test (with the Dunn's post hoc test) was applied for Fig 1D, Fig S4; the chi-squared test was applied for Fig 6A, Fig S3 (upper panels). All quantifications were performed on >3 independent experiments to account for technical variability. The size of the population (n) is presented directly in each figure legend. As presented in the figures, the differences between experimental groups are significant for * $P<0.05$; ** $P<0.01$, *** $P<0.001$ and **** $P<0.0001$.

***Study approval.*** Experiments on zebrafish were conducted prior to 5 days post fertilization, which corresponds to the non-autonomous stage of the animals and does not require specific authorization accordingly to the Directive 2010/63/EU. We obtained the approval of the ethical committee and the French ministry (reference N°036) for the creation of the new zebrafish line.

## AUTHOR CONTRIBUTIONS

Conceptualization and supervision: B.P.; Investigation: M.K. and A.Y. performed most of the experiments; L.L. realized the experiments concerning the genetic *gan* line; B.A. determined the spatio-temporal expression of z-gigaxonin; and R.M. performed the bioinformatics analysis and the rescue experiments; Discussions and scientific input: Ro.M.; Writing: B.P. with contribution from M.K. A.Y. and L.L.; Review and editing: B.P.


## ACKNOWLEDGMENTS

We are grateful to P. Beachy for providing the Shh-Light2 and ShhN cell lines; A. Schier and P. Huang for the *ptch2* probe. We thank C. Conan for formatting the movies on zebrafish; the CRBM zebrafish facility (Montpellier) and B. Delaval for the coordination of housing and kind support; P. Richard, M. Plays and N. Cubedo for zebrafish husbandry and assistance in injection; the MRI-COMET facility (C. Cazevieille, Montpellier) for electron microscopy, Y. Talmat-Amar for assisting in the preparation of samples for electron microscopy, S. Venteo for advice on in situ hybridization. We are also grateful to the IGF institute (Montpellier) and especially C. Joplin and A. Faucherre for the provision of the Zebrabox, Carl Zeiss for the LightSheet Z.1 microscope and N. Tricaud for the confocal laser-scanning microscope. This work was funded by l'Institut National de la Santé et de la Recherche Médicale (INSERM) to B .P., l'Association Française contre les Myopathies (AFM) to A.Y. and the Fondation pour la Recherche Médicale (FRM) to M.K., L.L. and B.A.; B. P. is supported by grants from the ATIP-Avenir program (INSERM), the AFM and the Fondation Maladies Rares (FMR). We are very grateful to J. Hazan for scientific discussions, S. Schneider-Maunoury, H. Gilbreath, P. Carroll and G. Campbell for critical reading and comments on the manuscript, K. Loulier and F. Michon for helpful discussion during the revision.

## REFERENCES


1. DiFiglia M, et al. Huntingtin is a cytoplasmic protein associated with vesicles in human and rat brain neurons. *Neuron.* 1995;14(5):1075-1081.
2. Kimberly WT, Zheng JB, Town T, Flavell RA, Selkoe DJ. Physiological regulation of the beta-amyloid precursor protein signaling domain by c-Jun N-terminal kinase JNK3 during neuronal differentiation. *J Neurosci.* 2005;25(23):5533-5543.
3. Lorent K, Overbergh L, Moechars D, De Strooper B, Van Leuven F, Van den Berghe H. Expression in mouse embryos and in adult mouse brain of three members of the amyloid precursor protein family, of the alpha-2-macroglobulin receptor/low density lipoprotein receptor-related protein and of its ligands apolipoprotein E, lipoprotein lipase, alpha-2-macroglobulin and the 40,000 molecular weight receptor-associated protein. *Neuroscience.* 1995;65(4):1009-1025.
4. Paulsen JS, et al. Brain structure in preclinical Huntington's disease. *Biol Psychiatry.* 2006;59(1):57-63.
5. Reiman EM, et al. Brain imaging and fluid biomarker analysis in young adults at genetic risk for autosomal dominant Alzheimer's disease in the presenilin 1 E280A kindred: a case-control study. *Lancet Neurol.* 2012;11(12):1048-1056.
6. Milnerwood AJ, Raymond LA. Corticostriatal synaptic function in mouse models of Huntington's disease: early effects of huntingtin repeat length and protein load. *J Physiol.* 2007;585(Pt 3):817-831.
7. Young-Pearse TL, Bai J, Chang R, Zheng JB, LoTurco JJ, Selkoe DJ. A critical function for beta-amyloid precursor protein in neuronal migration revealed by in utero RNA interference. *J Neurosci.* 2007;27(52):14459-14469.
8. Liu H, Shafey D, Moores JN, Kothary R. Neurodevelopmental consequences of Smn depletion in a mouse model of spinal muscular atrophy. *J Neurosci Research.* 2010;88(1):111-122.
9. Molero AE, Gokhan S, Gonzalez S, Feig JL, Alexandre LC, Mehler MF. Impairment of developmental stem cell-mediated striatal neurogenesis and pluripotency genes in a knock-in model of Huntington's disease. *Proc Natl Acad Sci U S A.* 2009;106(51):21900-21905.
10. Molina-Calavita M, Barnat M, Elias S, Aparicio E, Piel M, Humbert S. Mutant huntingtin affects cortical progenitor cell division and development of the mouse neocortex. *J Neurosci.* 2014;34(30):10034-10040.
11. Molero AE, et al. Selective expression of mutant huntingtin during development recapitulates characteristic features of Huntington's disease. *Proc Natl Acad Sci U S A.* 2016;113(20):5736-5741.
12. Berg BO, Rosenberg SH, Asbury AK. Giant axonal neuropathy. *Pediatrics.* 1972;49(6):894-899.
13. Johnson-Kerner BL, Roth L, Greene JP, Wichterle H, Sproule DM. Giant axonal neuropathy: An updated perspective on its pathology and pathogenesis. *Muscle Nerve.* 2014;50(4):467-476.
14. Kuhlenbaumer G, Timmerman V, Bomont P. In: Pagon RA, et al. eds. GeneReviews® [Internet]. Seattle (WA): University of Washington, Seattle; 1993-2019.
15. Bomont P, et al. The gene encoding gigaxonin, a new member of the cytoskeletal BTB/kelch repeat family, is mutated in giant axonal neuropathy. *Nat Genet.* 2000;26(3):370-374.
16. Demir E, et al. Giant axonal neuropathy: clinical and genetic study in six cases. *J Neurol Neurosurg Psychiatry.* 2005;76(6):825-832.

17. Ganay T, Boizot A, Burrer R, Chauvin JP, Bomont P. Sensory-motor deficits and neurofilament disorganization in gigaxonin-null mice. *Mol Neurodegener.* 2011;6:25.
18. Furukawa M, He YJ, Borchers C, Xiong Y. Targeting of protein ubiquitination by BTB-Cullin 3-Roc1 ubiquitin ligases. *Nat Cell Biol.* 2003;5(11):1001-1007.
19. Boizot A, et al. The instability of the BTB-KELCH protein Gigaxonin causes Giant Axonal Neuropathy and constitutes a new penetrant and specific diagnostic test. *Acta Neuropathol Commun.* 2014;2:47.
20. Bomont P. Degradation of the Intermediate Filament Family by Gigaxonin. *Methods Enzymol.* 2016;569:215-231.
21. Prineas JW, Ouvrier RA, Wright RG, Walsh JC, McLeod JG. Giant axonal neuropathy: a generalized disorder of cytoplasmic microfilament formation. *J Neuropathol Exp Neurol.* 1976;35(4):458-470.
22. Dequen F, Bomont P, Gowing G, Cleveland DW, Julien JP. Modest loss of peripheral axons, muscle atrophy and formation of brain inclusions in mice with targeted deletion of gigaxonin exon 1. *J Neurochem.* 2008;107(1):253-264.
23. Israeli E, et al. Intermediate filament aggregates cause mitochondrial dysmotility and increase energy demands in giant axonal neuropathy. *Hum Mol Genet.* 2016;25(11):2143-2157.
24. Mahammad S, et al. Giant axonal neuropathy-associated gigaxonin mutations impair intermediate filament protein degradation. *J Clin Invest.* 2013;123(5):1964-1975.
25. Bomont P, Koenig M. Intermediate filament aggregation in fibroblasts of giant axonal neuropathy patients is aggravated in non dividing cells and by microtubule destabilization. *Hum Mol Genet.* 2003;12(8):813-822.
26. Cleveland DW, Yamanaka K, Bomont P. Gigaxonin controls vimentin organization through a tubulin chaperone-independent pathway. *Hum Mol Genet.* 2009;18(8):1384-1394.
27. Johnson-Kerner BL, et al. Intermediate filament protein accumulation in motor neurons derived from giant axonal neuropathy iPSCs rescued by restoration of gigaxonin. *Hum Mol Genet.* 2015;24(5):1420-1431.
28. Scrivo A, Codogno P, Bomont P. Gigaxonin E3 ligase governs ATG16L1 turnover to control autophagosome production. *Nat Commun.* 2019;10(1):780.
29. Ingham PW, McMahon AP. Hedgehog signaling in animal development: paradigms and principles. *Genes Dev.* 2001;15(23):3059-3087.
30. Jessell TM. Neuronal specification in the spinal cord: inductive signals and transcriptional codes. *Nat Rev Genet.* 2000;1(1):20-29.
31. Te KG, Reggiani C. Skeletal muscle fibre type specification during embryonic development. *J Muscle Res Cell Motil.* 2002;23(1):65-69.
32. Bale AE. Hedgehog signaling and human disease. *Annu Rev Genomics Hum Genet.* 2002;3:47-65.
33. Jiang J, Hui CC. Hedgehog signaling in development and cancer. *Dev Cell.* 2008;15(6):801-812.
34. Briscoe J, Therond PP. The mechanisms of Hedgehog signalling and its roles in development and disease. *Nat Rev Mol Cell Biol.* 2013;14(7):416-429.
35. Wheway G, Nazlamova L, Hancock JT. Signaling through the Primary Cilium. *Front Cell Dev Biol.* 2018;6:8.
36. Haycraft CJ, Banizs B, Aydin-Son Y, Zhang Q, Michaud EJ, Yoder BK. Gli2 and Gli3 localize to cilia and require the intraflagellar transport protein polaris for processing and function. *PLoS Genet.* 2005;1(4):e53.
37. Huangfu D, Anderson KV. Cilia and Hedgehog responsiveness in the mouse. *Proc Natl Acad Sci U S A.* 2005;102(32):11325-11330.

38. Jiang J. Regulation of Hh/Gli signaling by dual ubiquitin pathways. *Cell cycle.* 2006;5(21):2457-2463.
39. Li T, et al. Ubr3, a Novel Modulator of Hh Signaling Affects the Degradation of Costal-2 and Kif7 through Poly-ubiquitination. *PLoS Genet.* 2016;12(5):e1006054.
40. Schweiger S, et al. The E3 ubiquitin ligase MID1 catalyzes ubiquitination and cleavage of Fu. *J Biol Chem.* 2014;289(46):31805-31817.
41. Zhou Z, et al. Deubiquitination of Ci/Gli by Usp7/HAUSP Regulates Hedgehog Signaling. *Dev Cell.* 2015;34(1):58-72.
42. Huang S, et al. Activation of Smurf E3 ligase promoted by smoothened regulates hedgehog signaling through targeting patched turnover. *PLoS biology.* 2013;11(11):e1001721.
43. Yue S, et al. Requirement of Smurf-mediated endocytosis of Patched1 in sonic hedgehog signal reception. *Elife.* 2014;3.
44. Chen XL, et al. Patched-1 proapoptotic activity is downregulated by modification of K1413 by the E3 ubiquitin-protein ligase Itchy homolog. *Mol Cell Biol.* 2014;34(20):3855-3866.
45. Lewis KE, Eisen JS. From cells to circuits: development of the zebrafish spinal cord. *Prog Neurobiol.* 2003;69(6):419-449.
46. Chen W, Burgess S, Hopkins N. Analysis of the zebrafish smoothened mutant reveals conserved and divergent functions of hedgehog activity. *Development.* 2001;128(12):2385-2396.
47. Vanderlaan G, Tyurina OV, Karlstrom RO, Chandrasekhar A. Gli function is essential for motor neuron induction in zebrafish. *Dev Biol.* 2005;282(2):550-570.
48. Varga ZM, et al. Zebrafish smoothened functions in ventral neural tube specification and axon tract formation. *Development.* 2001;128(18):3497-3509.
49. Buysse K, et al. Giant axonal neuropathy caused by compound heterozygosity for a maternally inherited microdeletion and a paternal mutation within the GAN gene. *Am J Med Genet A.* 2010;152A(11):2802-2804.
50. Karlstrom RO, et al. Genetic analysis of zebrafish gli1 and gli2 reveals divergent requirements for gli genes in vertebrate development. *Development.* 2003;130(8):1549-1564.
51. Taipale J, et al. Effects of oncogenic mutations in Smoothened and Patched can be reversed by cyclopamine. *Nature.* 2000;406(6799):1005-1009.
52. Corbit KC, Aanstad P, Singla V, Norman AR, Stainier DY, Reiter JF. Vertebrate Smoothened functions at the primary cilium. *Nature.* 2005;437(7061):1018-1021.
53. Beattie CE, Hatta K, Halpern ME, Liu H, Eisen JS, Kimmel CB. Temporal separation in the specification of primary and secondary motoneurons in zebrafish. *Dev Biol.* 1997;187(2):171-182.
54. Aviles EC, Wilson NH, Stoeckli ET. Sonic hedgehog and Wnt: antagonists in morphogenesis but collaborators in axon guidance. *Front Cell Neurosci.* 2013;7:86.
55. Lee RT, Zhao Z, Ingham PW. Hedgehog signalling. *Development.* 2016;143(3):367-372.
56. De Mori R, et al. Hypomorphic Recessive Variants in SUFU Impair the Sonic Hedgehog Pathway and Cause Joubert Syndrome with Cranio-facial and Skeletal Defects. *Am J Hum Genet.* 2017;101(4):552-563.
57. Schimmenti LA, et al. Novel mutation in sonic hedgehog in non-syndromic colobomatous microphthalmia. *Am J Med Genet A.* 2003;116A(3):215-221.
58. Roessler E, at al. Mutations in the human Sonic Hedgehog gene cause holoprosencephaly. *Nat Genet.* 1996;14(3):357-360.

59. Rubino S, Qian J, Pinheiro-Neto CD, Kenning TJ, Adamo MA. A familial syndrome of hypothalamic hamartomas, polydactyly, and SMO mutations: a clinical report of 2 cases. *J Neurosurg Pediatr.* 2018;23(1):98-103.
60. Chen SD, Yang JL, Hwang WC, Yang DI. Emerging Roles of Sonic Hedgehog in Adult Neurological Diseases: Neurogenesis and Beyond. *Int J Mol Sci.* 2018;19(8).
61. Traiffort E, Angot E, Ruat M. Sonic Hedgehog signaling in the mammalian brain. *J Neurochem.* 2010;113(3):576-590.
62. Haeussler M, et al. Evaluation of off-target and on-target scoring algorithms and integration into the guide RNA selection tool CRISPOR. *Genome Biol.* 2016;17(1):148.
63. Angebault C, et al. Recessive Mutations in RTN4IP1 Cause Isolated and Syndromic Optic Neuropathies. *Am J Hum Genet.* 2015;97(5):754-760.
64. Zhao C. Hedgehog (Hh) reporter activity assay. *Bio-Protoc.* 2014;4(e1182).

Table 1. List of primers

| primers | | | |
|---|---|---|---|
| **PCR** | *gan* exons 2-3 | forward | 5'-AATTACAACCCACCAAAG-3' |
| | | reverse | 5'-GTCGAGGCTTCAGTGTCAT-3' |
| | *gan* exons 3-4 | forward | 5'-AGAAGCTCAACGTTGGGAA-3' |
| | | reverse | 5'-GCTCCTCCTAGAGACT-3' |
| **In situ hybridization** | *gan* antisense probe | forward * | 5'-AATTAACCCTCACTAAAGGGAGAgaaactcacggacatagtcgaa-3' |
| | | reverse | 5'- attgttgtatggagtctct-3' |
| | *gan* sense probe | forward * | 5'- AATTAACCCTCACTAAAGGGAGAattgttgtatggagtctcta-3' |
| | | reverse | 5'- gaaactcacggacatagt-3' |
| **Genotyping** | *gan* exon 1 | forward | 5'-CAGCACATCTGTCTGTACTGTG-3' |
| | | reverse | 5'-CAGCAGCTACTCATCTGATCTC-3' |
| | *gan* exon 11 | reverse | 5'-GCATCAAGATACTAGCCGTATC-3' |
| **Morpholino oligonucleotides** | *gan* | Mo ex2-3 | 5′- AGAGTGATCTACAGAAGGAAACAGT-3' |
| | *gan* | Mo ex1-2 | 5'-TTGGTCCTGGAAACACAGTAACACA-3 |
| | *gan* | Mis ex2-3 | 5′- AGAGTcATgTACAcAAGcAAACAcT-3′ |
| **Cloning in expressing vectors** | Gig | forward** | 5'–ggggacaagtttgtacaaaaaagcaggcttcATGTCAGACCCTAAAAGAGCT-3' |
| | | reverse | 5'– ggggaccactttgtacaagaaagctgggttTGTGGATGGAACCCGAATGCG-3' |
| | Ptch | forward** | 5'–ggggacaagtttgtacaaaaaagcaggcttcATGGCCTCGGCTGTTAATGT-3' |
| | | reverse | 5'–ggggaccactttgtacaagaaagctgggttGAGCCGTATTCTGAGTCTGT-3' |
| **Gene inactivation** | *GAN* | siRNA | 5'-P-UAUCCCUUCAAGUUCAAUCUU-3' |
| | Mis | siRNA | 5'-UAUCaCUUCAAGUcCAAUCUU-3' |

* upper case: T3 promoter sequence
**lower case: ATTB sequence

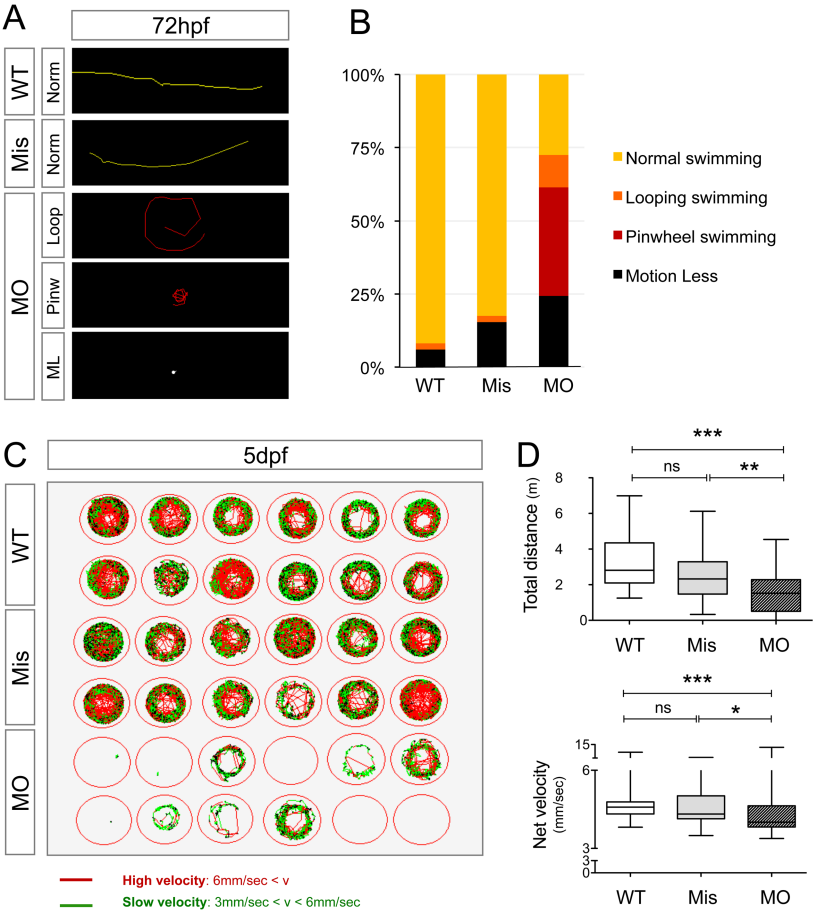


**Figure 1. Loss of motility in *gan* morphants**. (A) WT, Mis and MO-injected embryos were examined using the touch-response test at 72hpf. The swimming pattern was recorded as normal, motionless ("ML", absence of response), looping ("loop", circular trajectory) and pinwheel ("pinw") swimming (see Supplemental Movie 1). (B) Quantification of the percentage of embryos exhibiting the different motor behaviors in the control (n=139), Mis (n=66) and MO (n=60) populations. (C) Tracking analysis of the spontaneous locomotion at 5dpf. Red and green trajectories correspond to fast and slow swimming, respectively. Motility is abolished in 80% MO injected embryos. (D) Quantification of the covered distance (top panel) and net velocity (lower panel) during spontaneous locomotion at 5dpf. Statistics: in the absence of normality of distribution of the data, a Kruskal-Wallis test (Dunn's post hoc test) was applied; medians with interquartile range, min and max values are represented; n=48 (WT), n=48 (Mis), n=49 (MO); ns, not statistically significant; * $P<0.05$ ** $P<0.01$; *** $P<0.001$.

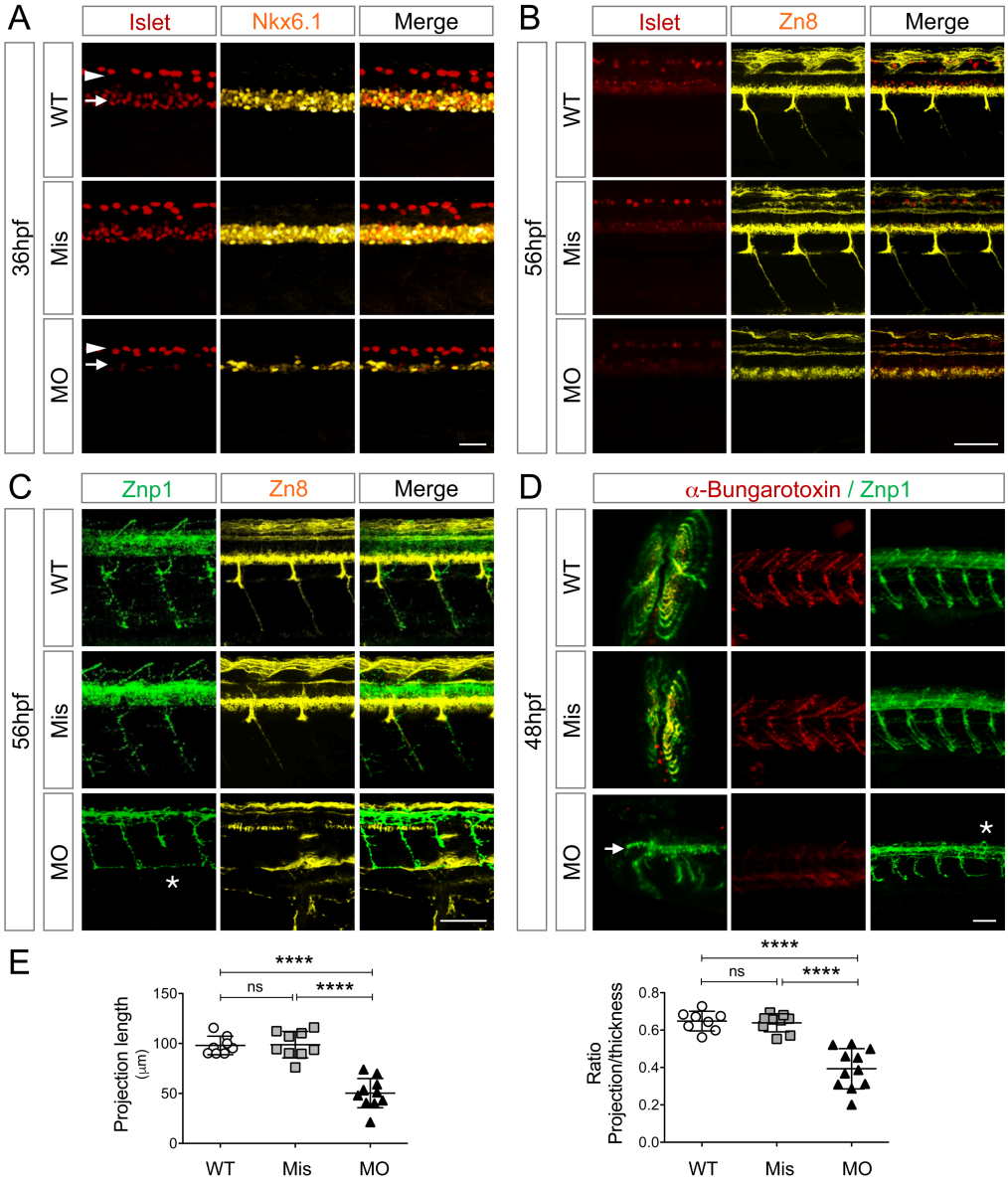


**Figure 2. Impaired MN specification, altered axonogenesis and neuromuscular junctions in *gan* morphants.** (A) Gigaxonin repression impairs late specification of motor neuron progenitors and differentiation of secondary motor neurons (sMN). Progenitors and motor neurons were visualized, respectively with Nkx6.1 and Islet immunostaining in a lateral view of spinal cord in WT, Mis and MO injected embryos, at 36hpf. Ventral Islet positive (Islet$^{+}$) cells correspond to motor neurons (arrow), dorsal Islet$^{+}$ cells correspond to the sensory Rohan-Beard neurons (arrowhead). In absence of gigaxonin, a large reduction in both Nkx6.1$^{+}$ MN progenitors and Islet$^{+}$ sMN is observed at 36hpf. (B-E) Gigaxonin depletion leads to abnormal architecture of pMN axons. (B) gigaxonin depletion leads to the absence of sMN cell bodies (Islet$^{+}$) and axons (Zn8$^{+}$) at 56hpf. (C) pMN axonal projections (Znp1$^{+}$) show abnormal arborization in morphants at 56hpf, with some CaP pMN axons exhibiting reduced length (white star). (D, left panel) Three dimensional examination of the spinal cord of gigaxonin-depleted embryos at 48hpf, using the LightSheet microscopy. Gigaxonin depletion leads to additional abnormalities in the spinal cord architecture: protruding axons (arrow), absence of the MiP and RoP motor axons (transverse view) (see Supplemental movies 2 and 3). (D, right panel) Neuromuscular junctions (α-bungarotoxin$^{+}$) and subsequent innervation of trunk muscles are abolished in *gan* morphants. Note that CaP axons are occasionally absent (white star). (E) Quantification of the mean length of the pMN CaP axons (left panel) and mean length relative to the body thickness of the embryos (as defined by phase contrast pictures, right panel) shows significant neurite abnormalities. Statistics: with normality of the distribution of the data, a one-way ANOVA test (Bonferroni post-hoc test) was used. Data represent mean ± SD; individual values are represented; n=8 (WT), n=9 (Mis), n=11 (MO); ns not statistically significant; **** $P$<0.0001. Scale Bar A: 25µm; B-D: 100µm.

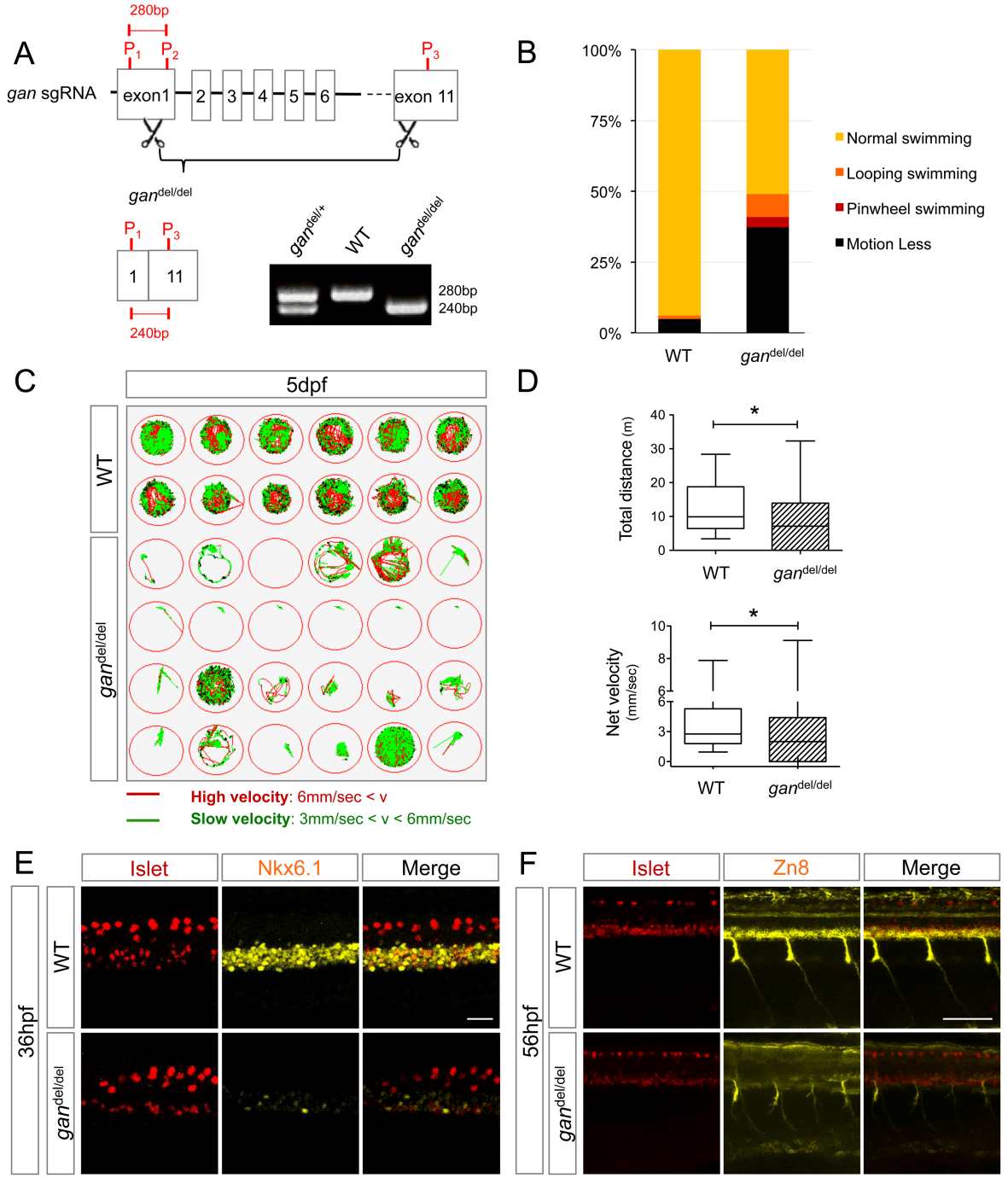


**Figure 3. The *gan*$^{del/del}$ zebrafish, similar to *gan* morphants, exhibits Shh-like deficits.** (A) Schematic representation of the deletion within the endogenous *gan* locus, and genotyping of the *gan*$^{del/del}$ line. (B-D) *gan*$^{del/del}$ embryos display locomotor deficits. (B) Quantification of the touch-evoked response of *gan*$^{del/del}$ embryos at 72hpf; n=82 (WT), n=110 (*gan*$^{del/del}$). (C) Tracking analysis of the spontaneous locomotion of 5dpf control and mutant larvae. (D) Quantification of total distance traveled (top panel) and net velocity (bottom panel) at 5dpf in the control (n=24) and *gan*$^{del/del}$ (n=64) populations. Statistics: in the absence of normality of distribution of the data, a two-tailed Mann Whitney test was applied; medians with interquartile range, min and max values are represented; * $P$<0.05. (E) Nkx6.1 immunostaining at 36hpf is significantly decreased in the mutant line in 85% of mutants (n=21 out of 25 analyzed embryos). (F) Zn8 immunostaining reveals a strong defect in sMN axonal projections at 56hpf in 72% of *gan*$^{del/del}$ mutants (n=18 out of 25 analyzed embryos). Scale bar in E: 25µm; Scale Bar in F: 100µm.

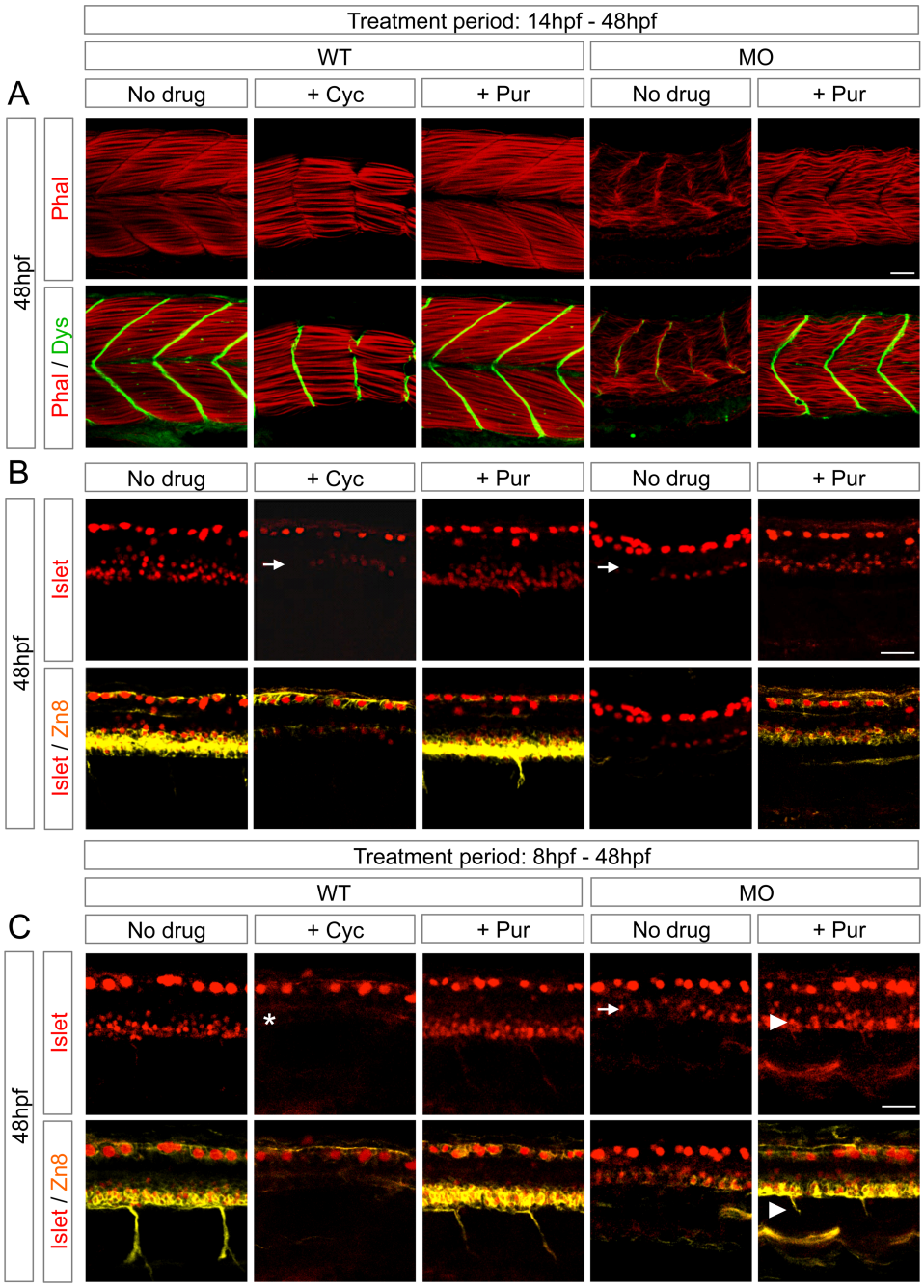


**Figure 4. Modulation of Shh activity mimics and restores gigaxonin-dependent phenotypes in zebrafish.** (A-B) Lateral view of WT and MO injected embryos at 48hpf after cyclopamine or purmorphamine treatment between 14-48hpf. (A) MO injection mimics the cyclopamine-induced loss-of-Shh phenotype (U-shape somites (Dystrophin$^{+}$) and less dense myofibers (Phalloidin$^{+}$), which is partially rescued with purmorphamine. (B) Using the same treatment regime, Islet/Zn8 immunostaining in cyclopamine-treated or MO embryos reveals a loss of sMN, while pMN are still visible (arrows). Purmorphamine treatment partially rescues the loss-of-Shh like phenotype in *gan* morphants. (C) Earlier Shh activation by purmorphamine from 8hpf, during the wave of pMN birth (as shown by absence of pMN in control embryos with cyclopamine: white star), is effective in reversing the defects in sMN specification in the *gan* morphant (arrowheads). Representative picture of (A) n=18/18 (WT), n=18/18 (WT+Cyc), n=18/18 (WT+Pur), n=18/18 (MO), n=5/21 (MO+Pur); (B) n=30/30 (WT), n=35/35 (WT+Cyc), n=30/30 (WT+Pur), n=35/35 (MO), n=7/40 (MO+Pur) and (C) n=56/56 (WT), n=49/49 (WT+Cyc), n=73/74 (WT+Pur), n=46/49 (MO), n=53/76 (MO+Pur). Scale Bar: 25µm.

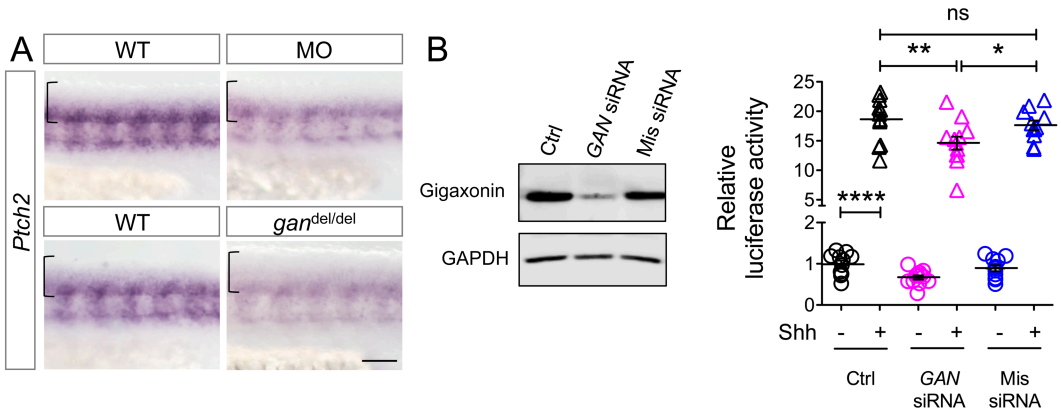


**Figure 5. Gigaxonin depletion induces a decrease in Shh activation in zebrafish and in a mammalian reporter cell line.** (A) Lateral view of zebrafish spinal cord at 32hpf showing a reduction of *ptch2* mRNA expression in both MO injected and *gan*$^{del/del}$ animals. Spinal cord is indicated by square brackets. (B) Quantification of Shh activation in Shh-Light2 cells depleted in gigaxonin. Left panel: transient knock-down of *GAN*, as revealed by immunoblotting. Right panel: Quantification of the luciferase activity in Shh-Light2 cells depleted in gigaxonin, with or without treatment with Shh-CM for 48h. In the absence of gigaxonin, the Shh-induced luciferase activity is diminished. Statistics: with normality of the distribution of the data, a one-way ANOVA test (with Bonferroni post-hoc test) was used, means ± SEM are represented; n=11-12 independent experiments, performed in triplicate; ns not statistically significant; * $P$<0.05, ** $P$<0.01 ; **** $P$<0.0001. Scale bar: 50 µm.

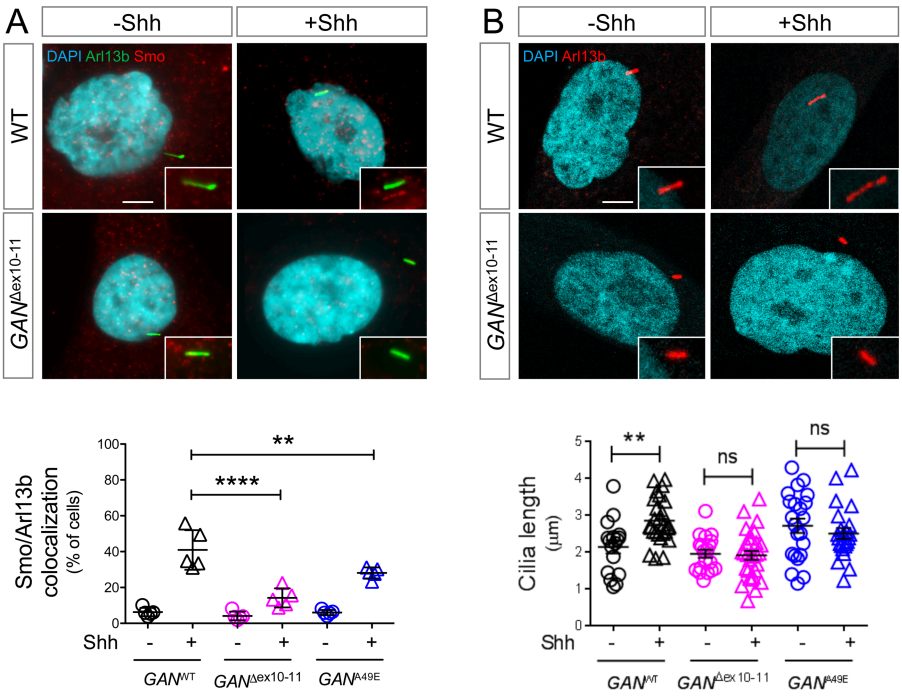


**Figure 6. Decreased responsiveness of primary fibroblasts from GAN patients to the activation of the Shh pathway.** (A) Shh-CM treatment for 4h causes translocation of Smo into the cilium (arl13b$^{+}$) in control but is greatly decreased in patient primary fibroblasts, bearing distinct mutations in the *GAN* gene: *GAN*$^{\Delta ex10\text{-}11}$ and *GAN*$^{A49E}$. Lower panel: quantification of the proportion of Smo$^{+}$ cilia in control and GAN fibroblasts, with or without Shh treatment. Statistics: proportions of experimental groups were compared with the Chi-squared test, data represent means ± SEM; n=419 (GAN$^{WT}$), n=410 (GAN$^{WT}$+Shh), n=179 (*GAN*$^{\Delta ex10\text{-}11}$), n=135 (*GAN*$^{\Delta ex10\text{-}11}$+Shh), n=295 (*GAN*$^{A49E}$), n=347 (*GAN*$^{A49E}$+Shh) from 5 independent experiments; ** $P$<0.01, **** $P$<0.0001 correspond to the comparison between patient and control cells in the presence of Shh (for information: pairwise comparisons of patient with control cells are not statistically significant in the absence of Shh). (B) Shh-CM treatment for 24h increases the length of primary cilia in control but not in *GAN*$^{\Delta ex10\text{-}11}$ and *GAN*$^{A49E}$ patient primary fibroblasts. Lower panel: quantification of the ciliary length in human fibroblasts, showing a significant increase upon Shh-CM stimulation in control but not mutant cells. Statistics: with normality of the distribution of the data, a one-way ANOVA test (with Bonferroni post-hoc test) was used, means ± SEM are represented; n=24 (*GAN*$^{WT}$), n=26 (*GAN*$^{WT}$+Shh), n=19 (*GAN*$^{\Delta ex10\text{-}11}$), n=28 (*GAN*$^{\Delta ex10\text{-}11}$+Shh), n=22 (*GAN*$^{A49E}$), n=23 (*GAN*$^{A49E}$+Shh); ns, not statistically significant; ** $P$<0.01. Scale bar: 10µm.

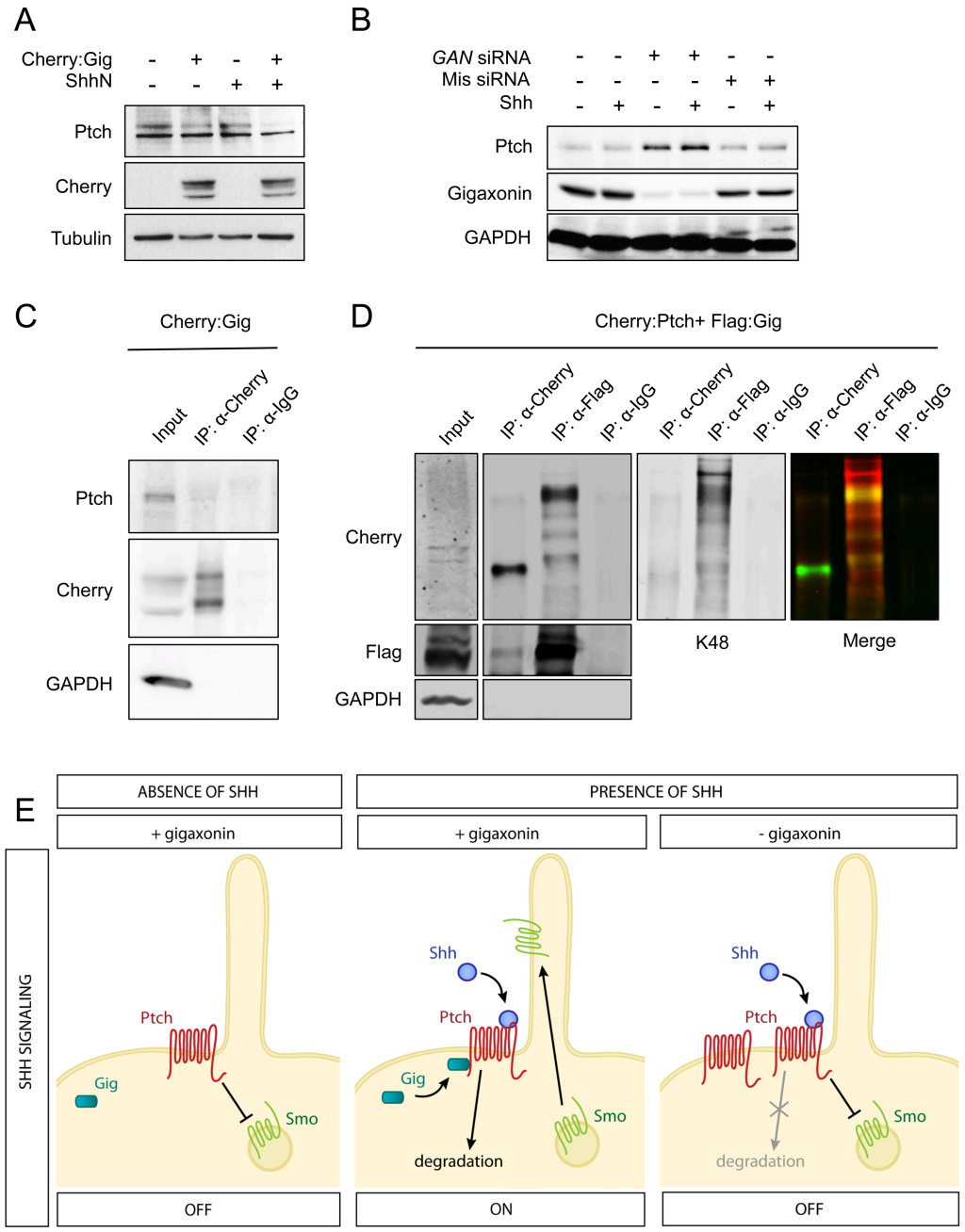


**Figure 7. Shh-dependent control of Ptch abundance by gigaxonin.** (A) NIH-3T3 cells were transfected with human Cherry-Gig plasmid ± 3ug/ml Shh for 48h. Degradation of endogenous Ptch protein occurs only in the presence of both ectopic gigaxonin and Shh. (B) Repression of the endogenous gigaxonin, using siRNA causes an increase of the endogenous Ptch levels in Shh-Light2 cells, which is potentiated by Shh induction. (C, D) Interaction between gigaxonin and Ptch, as revealed by reverse immunoprecipitation on both endogenous (C) and ectopic (D) Ptch protein. Shh-Light2 cells are transfected with human Cherry-Gig in (C); COS-7 cells are transfected with zebrafish 3Flag-Gig and zebrafish Cherry-Ptch in (D). IgG serves as an internal negative control. (D) Cherry immunoprecipitation identifies Ptch proteins which are mainly not modified, while the Ptch pool enriched in gigaxonin immunocomplex presents a laddering overlapping with K48 specific ubiquitin chain. (E) Model of action of the gigaxonin-E3 ligase in the initiation of Shh signaling. In an OFF state (left panel), prior to Shh activation, receiving cells silence the cascade through the inhibitory effect of the Ptch receptor on the effector Smo. Upon Shh production, the active Shh form is released and received by progenitor cells. Gigaxonin acts as an initiator of signal transduction by degrading Shh-bound Ptch receptor (middle panel), hence allowing the derepression of the signal transducer Smo, which translocates into the cilium to activate the pathway. In absence of gigaxonin (right panel), receiving tissues are unable to interpret Shh signaling, due to the constitutive repression of Smo induced by the accumulation of Shh-bound Ptch receptor.